

Flow-Guided Diffusion for Video Inpainting

Bohai Gu^{1,4*} Yongsheng Yu^{2*} Heng Fan³ Libo Zhang^{1,4†}

¹ Institute of Software Chinese Academy of Sciences, Beijing, China

² University of Rochester, New York, USA

³ University of North Texas, Denton TX, USA

⁴ University of Chinese Academy of Sciences, Beijing, China

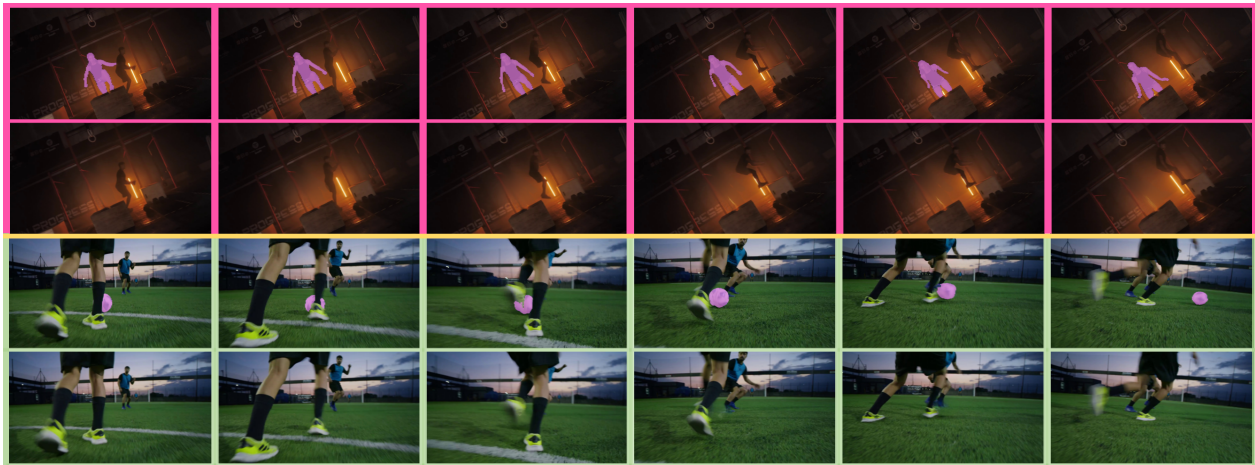


Figure 1. Our FGDVI utilizes flow-guided diffusion for video inpainting, excelling in scenarios with substantial motion and darkness.

Abstract

*Video inpainting has been challenged by complex scenarios like large movements and low-light conditions. Current methods, including emerging diffusion models, face limitations in quality and efficiency. This paper introduces the **Flow-Guided Diffusion model for Video Inpainting (FGDVI)**, a novel approach that significantly enhances temporal consistency and inpainting quality via reusing an off-the-shelf image generation diffusion model. We employ optical flow for precise one-step latent propagation and introduces a model-agnostic flow-guided latent interpolation technique. This technique expedites denoising, seamlessly integrating with any Video Diffusion Model (VDM) without additional training. Our FGDVI demonstrates a remarkable 10% improvement in flow warping error E_{warp} over existing state-of-the-art methods. Our comprehensive experiments validate superior performance of FGDVI, offering a promising direction for advanced video inpainting. The code and detailed results will be publicly available in <https://github.com/NevSNeve/FGDVI>.*

*Bohai Gu and Yongsheng Yu contributed equally to this work. †Corresponding author: Libo Zhang (libo@iscas.ac.cn).

1. Introduction

Video inpainting aims at guaranteeing the integrity of content within each frames, while handle the inter-frame temporal dynamics, which plays an essential role in computer vision such as object removal [7], logo removal [43], video restoration [34], and watermark removal [23].

The objective of video inpainting method is to shift pixels across frames while hallucinating deficient [25, 47] pixels. Existing approaches [18, 50, 54] adopt end-to-end transformers within optical flow module for temporal consistent. However, they often result in blurred or mosaic-like outcomes for deficient pixels, even with the use of a discriminator supervising [20, 49]. video inpainting remains a persistent problem that may benefit from stronger solutions, such as leveraging image models as a generative prior.

While image inpainting has seen impressive advances [24, 35, 45, 46, 48], particularly with diffusion models. Diffusion model [11, 30, 33] is capable of generating realistic content [27, 37, 55]. The process of iterative sampling allows for easier integration of control signals [10, 51] and the reconstruction of more fine-grained details. However, the extra time dimension in video inpainting demands preserving temporal consistency and accounting

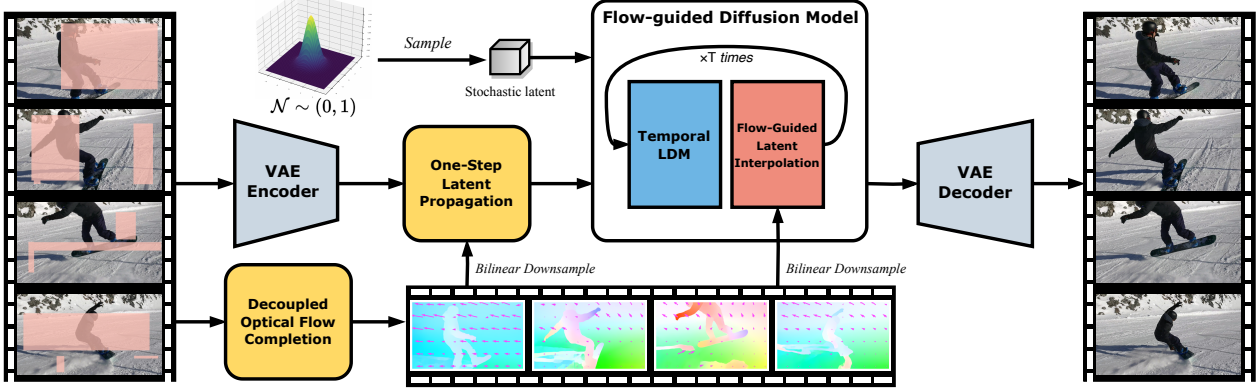


Figure 2. Overview of the flow-guided diffusion model. The VAE and flow completion module are fixed during training.

for the complex motion, which is different from image inpainting. The embarrassment lies in the extensive inference time of diffusion models in multi-step reasoning, which remains inefficient for video despite advancements in existing acceleration techniques [5, 22, 33]. Therefore, employing a well-trained diffusion model as a prior is a non-trivial challenge.

To address the issues mentioned, we hypothesize that adjacent video frames should share a similar sampling knowledge. In this paper, we take one step further by using optical flow to propagate latent-level features, reducing the number of frames that require denoising while maintaining temporal consistency. Specifically, we propose a novel flow-guided latent interpolation approach for diffusion-based denoising. Instead of inferring the latent codes for each frame at every time step [4, 12, 32], we aim to infer a subset of latent codes and then propagate these as the latent codes for the remaining via optical flow warping.

By equipping a pre-trained unconditional image generation diffusion model with optical flow, we present a holistic framework, the **Flow-Guided Diffusion** model for **Video Inpainting** (FGDVI). In particular, we adopt the latent diffusion model [30] and design series of modules to harness optical flow. To process optical flow from masked frame inputs, we utilize an decoupled flow completion module to predict and mend the flow. Moreover, a dedicated one-step latent propagation module is designed to inpaint corrupted video frames under with guidance of the reconstructed flow. The completed flow also plays a role in latent interpolation to efficiently propagate information through a simple yet effective warping operation. To unlock the capabilities of the pretrained image diffusion model for video, we also incorporate spatiotemporal attention networks into its U-Net architecture. We carry out extensive experiments for object removal and free-form video inpainting in terms of both quantitative and qualitative evaluations. In summary, our paper contributes significantly in the following ways:

- We are the first to reveal the effectiveness of a diffusion-based method in video inpainting, achieving comparable performance with state-of-the-art methods. Our proposed FGDVI leverages optical flow to notably improve inpainting quality and temporal consistency, especially achieving a large margin of **10%** enhancement in flow warping error E_{warp} [17].
- We propose a model-agnostic flow-guided latent interpolation method to accelerate denoising sampling, which can be integrated into any video diffusion model (VDM). Compared to the vanilla diffusion, our approach significantly boosts inference speed by approximately **29%**.

2. Related Works

Video inpainting. Video inpainting has advanced significantly, primarily through transformer solutions and flow-guided methods. STTN [49] employs spatiotemporal attention for consistent content recovery, while DSTT [21] alternates spatial and temporal attention to mitigate memory intensity. Liu et al. [20] introduced a sophisticated Transformer, utilizing soft split and composite operations for enhanced results. Given the relative ease of completing flows compared to intricate RGB content filling [42], numerous methods [9, 14, 18, 42, 50, 54] employ completed flows for inpainting assistance. Typically, flow-based approaches encompass three phases: flow completion, content propagation, and content hallucination. Specifically, FGVC [9] integrates gradient propagation in content propagation, while E2FGVI [18] introduces an end-to-end flow completion module with a window-based transformer for content hallucination. FGT [50] combines decoupled spatiotemporal attention with FGVC’s gradient propagation. ProPainter [54] advances this field by merging dual-domain propagation with a mask-guided transformer.

Diffusion Model. Diffusion models (DMs) [11, 30, 33] hold particular advantages; they provide a robust and scalable training objective and typically yield more realis-

tic textures compared to end-to-end transformer-based approaches. Advancements in image processing have outpaced those in video modeling. To mitigate the significant costs, in video generation, the use of latent diffusion [30] is common. PDVM [44] transforms the latent 3D structure of videos into a trio of 2D, image-reminiscent latent spaces. Meanwhile, MagicVideo [53] incorporates a straightforward adaptor following the 2D convolutional layer. Latent-Shift [2] utilizes parameter-free temporal shift module to facilitate the transfer of information between frames. In contrast to them, our proposed optical flow-guided latent interpolation technique significantly reduces the cost of video inferencing without compromising on quality.

Existing and concurrent diffusion-based studies, such as M3DDM [8], also employ pre-trained LDM for video out-painting task but are hindered by the high cost of training. In contrast, our FGDVI, has been trained using just three GPUs. Additionally, two video editing methods, MagicEdit [19] and VideoComposer [38], have demonstrated proficiency in text-guided video completion. However, these approaches are not specialized in video inpainting and do not yet present state-of-the-art results.

3. Preliminaries

LDMs leverage a pretrained Variational Autoencoder (VAE) to operate in the latent space instead of pixel space. The diffusion forward process is imposing noise on a clean latent \mathbf{z}_0 for T times. A property of the forward process is that it admit sampling \mathbf{z}^t at random timestep t :

$$q(\mathbf{z}^t | \mathbf{z}^0) = \mathcal{Q}(\mathbf{z}^0, t) = \mathcal{N}(\mathbf{z}^t; \sqrt{\alpha_t} \mathbf{z}^0, (1 - \alpha_t) \mathbf{I}), \quad (1)$$

where $\alpha_t = \prod_{s=1}^t 1 - \beta_s$, β_s is the variance schedule for the timestep s , and we use $\mathcal{Q}(\cdot, \cdot)$ to represent this one-step noising process. The backward process applies a trained U-Net ϵ_θ for denoising: $p_\theta(\mathbf{z}_{t-1} | \mathbf{z}_t) = \mathcal{N}(\mathbf{z}_{t-1}; \mu_\theta(\mathbf{z}_t, t), \Sigma_\theta(\mathbf{z}_t, t))$, where distribution parameters μ_θ and Σ_θ are computed by the denoising model θ . To train a conditional LDM, the objective is given by:

$$\arg \min_{\theta} \mathbb{E}_{\mathbf{z}, \epsilon \sim \mathcal{N}(0, 1), t, c} [\|\epsilon - \epsilon_\theta(\mathbf{z}_t, t, c)\|_2^2], \quad (2)$$

where $\epsilon_\theta(\mathbf{z}_t, t, c)$ is the predicted noise based on \mathbf{z}_t , the time step t and the condition c . Once trained, we could leverage the deterministic sampling of DDIM [11] to denoise \mathbf{z}_t :

$$\begin{aligned} \mathbf{z}_{t-1} = \sqrt{\alpha_{t-1}} & \underbrace{\hat{\mathbf{z}}_{t \rightarrow 0}}_{\text{predicted } 'z_0'} + \\ & \underbrace{\sqrt{1 - \alpha_{t-1} - \sigma_t^2} \epsilon_\theta(\mathbf{z}_t, t, c)}_{\text{direction pointing to } \mathbf{z}_t} + \underbrace{\sigma_t \epsilon_t}_{\text{random noise}}, \end{aligned} \quad (3)$$

where σ_t are hyperparameters. The term $\mathbf{z}_{t \rightarrow 0}^t$ represents the predicted \mathbf{z}_0 at time step t , which is characterized

through the operation $\mathcal{P}(\cdot, \cdot)$, as delineated in the equation below. For conciseness and to circumvent any potential confusion with the concept of optical flow, we subsequently refer to $\hat{\mathbf{z}}_{t \rightarrow 0}$ as $\hat{\mathbf{z}}_0$. The precise formulation is as follows:

$$\hat{\mathbf{z}}_0 = \mathcal{P}(\mathbf{z}_t, \epsilon_\theta) = (\mathbf{z}_t - \sqrt{1 - \alpha_t} \epsilon_\theta(\mathbf{z}_t, t, c)) / \sqrt{\alpha_t}, \quad (4)$$

4. Method

Given a corrupted video sequence represented as $\mathbf{x} = \{\mathbf{x}_0, \mathbf{x}_1, \dots, \mathbf{x}_N\}$ with dimensions $\mathbb{R}^{N \times 3 \times H \times W}$, consisting of N frames, we process this input alongside its associated binary mask sequence $\mathbf{m} = \{\mathbf{m}_0, \mathbf{m}_1, \dots, \mathbf{m}_N\}$ in $\mathbb{R}^{N \times 1 \times H \times W}$. The corruption in \mathbf{x} is modeled by the Hadamard product (\odot) of the original video \mathbf{y} and the mask \mathbf{m} , resulting in $\mathbf{x} = \mathbf{y} \odot \mathbf{m}$. Our FGDVI aims to generate a set of spatio-temporally consistent inpainted video frames.

4.1. Turning Static Latents into Video Inpainter

Our pipeline initiates by encoding the masked video into frame-wise latent representations, aimed at reducing the inference burden. This process is denoted as $\mathcal{E}(\mathbf{x}) = \mathbf{z}_\phi \in \mathbb{R}^{N \times C \times H_\downarrow \times W_\downarrow}$, where the encoded latent reduces dimensionality, and $(H_\downarrow, W_\downarrow)$ denotes the spatial dimensions $(\frac{H}{4}, \frac{W}{4})$ of the encoded latent space. C represents the number of latent channels. In this context, and \mathcal{E} refers to the VAE encoder, and the decoder \mathcal{D} serves as its left inverse.

Our key insight for efficiently training a video inpainting model is to re-use a pre-trained, fixed unconditional LDM. We adopt θ_ψ to represent spatial self-attention layers of LDM, which is parameterized by parameter θ . However, due to a lack of temporal modeling, while the model can produce high-quality individual frames, using it to directly render a video with T consecutive frames fails. We therefore introduce spatiotemporal attention neural network layers θ_τ , to supplant spatial self-attention layers θ_ψ of U-Net. These are designed to learn coherent spatiotemporal transformations for filling in missing regions. Our temporal LDM circumvents the bulky 3D convolution layers. For visualization, see the right part of Figure 3. Specifically, the original spatial LDM treats the video as a collection of independent images, tokenizing them into n patches with a window size of (h, w) prior to the spatial attention layers. In contrast, our spatiotemporal layers shift the temporal axis into the patch dimension and then reshape it back into the video dimension as follows:

$$\begin{aligned} \mathbf{z} & \leftarrow \text{rearrange}(\mathbf{z}, (b \ t) \ n \ (h \ w) \rightarrow b \ n \ (t \ h \ w)) \\ \mathbf{z} & \leftarrow \theta_\tau(\mathbf{z}) \\ \mathbf{z} & \leftarrow \text{rearrange}(\mathbf{z}, b \ n \ (t \ h \ w) \rightarrow (b \ t) \ n \ (h \ w)), \end{aligned}$$

where we employ `rearrange` from the einops notation [29] to denote dimension transposition. For clarity, we

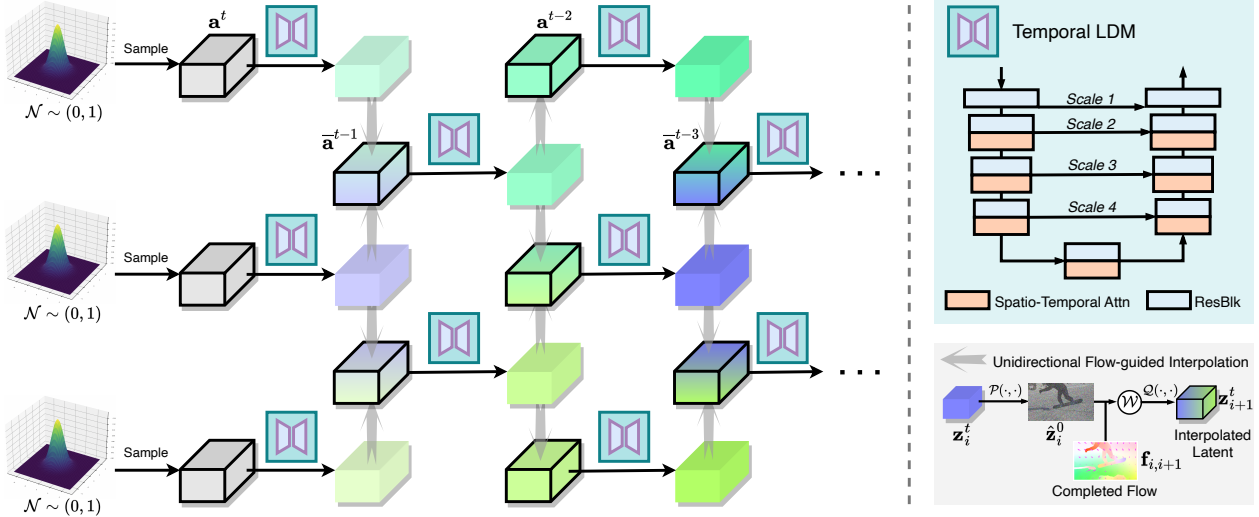


Figure 3. Process of the Flow-based Interpolation (left), temporal LDM and unidirectional interpolation (right).

add a batch dimension b and designate τ to represent the time dimension.

To get seamless content for masked image, blend noisy latent with unmasked region [3] at each denoising steps is straightforward for image generation model. But it falls short in lacks of spacial awareness of uncorrupted area while generation. We concatenated video latent \mathbf{z}_ϕ and binary mask \mathbf{m} with stochastic latent code \mathbf{z}_0 along channel axis as input of LDM, as in Fig. 2. Despite this concatenated input no longer fits the original distribution of LDM, we find that its intrinsic pattern can be revealed by finetuning.

We fix the VAE modules and train the temporal LDM using the same noise schedule as the base image model. Our denoising criterion, as shown in Equation 2, is termed $\mathcal{L}_{\text{diff}}$. Additionally, we impose an L1 loss at the latent level of $\mathcal{E}(\mathbf{I})$ for reconstruction, denoted as $\mathcal{L}_{\text{rec}} = \|\hat{\mathbf{z}}_{t \rightarrow 0}, \mathcal{E}(\mathbf{I})\|_1$, where $\hat{\mathbf{z}}_{t \rightarrow 0}$ represents the estimated \mathbf{z}_0 at an intermediate timestep as in Equation 4. The overall diffusion loss $\mathcal{L}_{\text{inpaint}}$ is given as follows:

$$\mathcal{L}_{\text{inpaint}} = \mathcal{L}_{\text{diff}} + \mathcal{L}_{\text{rec}}. \quad (5)$$

4.2. Flow Completion and Latent Propagation

In video inpainting, it's simpler to fill masked regions using optical flow rather than hallucinating RGB pixels from scratch. And employing flow for pixel propagation aids in maintaining natural temporal consistency [42]. To achieve this goal, we partition the flow process into two parts as described in Sec. 4.2.1 and Sec. 4.2.2, which acquiring a complete flow field for corrupted videos and imposing propagation to decrease the pressure of video inpainting.

4.2.1 Decoupled Optical Flow Completion

To represent the varying motion direction and velocity of objects over time for masked videos, previous methods [18, 31] have trained flow completion networks together with inpainting-oriented loss functions. However, they may lead to a suboptimal learning process and result in less precise completed flows [54]. Therefore, we decouple the stages of optical flow completion and inpainting in our methodology.

We utilize a swift ($< 0.01\text{s/flow}$) model for flow estimation, executed end-to-end, and initialized with the pre-trained SpyNet [28] checkpoint. Prior to predicting flow, we downscale the corrupted frames \mathbf{x} , to a quarter resolution, aligning with the latent code \mathbf{z} dimensions. For refining the model towards flow completion, which entails generating bidirectional completed optical flow, we conduct training on the same dataset with diffusion. The optical flow loss, inspired by prior work [18], is defined as:

$$\mathbb{E}_{i \in \mathcal{I}, j \in \mathcal{J}} \left[\|\hat{\mathbf{f}}_{i,i+1} - \mathbf{f}_{i,i+1}\|_1 + \|\hat{\mathbf{f}}_{j,j-1} - \mathbf{f}_{j,j-1}\|_1 \right], \quad (6)$$

where $\mathcal{I} = \{1, \dots, N-1\}$ and $\mathcal{J} = \{2, \dots, N\}$ signify the index sets for forward and backward temporal directions, respectively. Here, $\hat{\mathbf{f}}_{i,i+1}$ and $\mathbf{f}_{i,i+1}$ are the predicted and true forward flows between consecutive frames, while $\hat{\mathbf{f}}_{j,j-1}$ and $\mathbf{f}_{j,j-1}$ denote the backward flows. Further details will be elaborated in the experimental section 5.

4.2.2 One-step Latent Propagation

Although content can now be propagated using complete flows in image [54] or feature spaces [18], the repeated process of aggregating flows across frames [42, 50] is time-consuming. Alternatively mechanism like E²FGVI [18] and

ProPainter [54] performs propagation at the feature level between adjacent frames, but that is only suitable for end-to-end workflows. It is not compatible with diffusion models, which require iterating a U-Net over T timesteps (see Figure 2), rendering these existing methods computationally expensive. To address this, we propose a one-step latent propagation that shifts information in the latent space. This approach enhances encoded frames \mathbf{z}_ϕ prior to feeding the U-Net, thereby reducing the need to just a single propagation instead of T . Differing from previous methods [18, 42, 50, 54], our approach strikes efficiency for diffusion models while maintaining flow coherence.

As illustrated in Figure 4, for adjacent frame latent codes $\mathbf{z}_i, \mathbf{z}_j$, we initially warp \mathbf{z}_j using the complete optical flow $\hat{\mathbf{f}}_{i,j}$ to align it with the i -th frame, yielding the warped backward propagation latent. We concatenate it with the i -th frame’s latent code \mathbf{z}_i , mask \mathbf{m}_i , and flow $\hat{\mathbf{f}}_{i,j}$. Subsequently, we apply a series of convolutions to compute the offset $\mathbf{o}_{i \rightarrow j}$ and modulation weight $\mathbf{w}_{i \rightarrow j}$:

$$\mathbf{o}_{i \rightarrow j}, \mathbf{w}_{i \rightarrow j} = \text{Conv}(\mathcal{W}(\mathbf{z}_j, \hat{\mathbf{f}}_{i,j}), \hat{\mathbf{f}}_{i,j}, \mathbf{z}_i, \mathbf{m}_i), \quad (7)$$

where \mathcal{W} denotes the warping operation. In line with the approaches [18, 54], our method also incorporates flow-guided deformable convolution $\mathcal{D}(\cdot)$ to enhance alignment during latent propagation:

$$\hat{\mathbf{z}}_i = \text{Conv}(\mathcal{D}(\hat{\mathbf{z}}_j | \mathbf{o}_{i \rightarrow j}, \mathbf{w}_{i \rightarrow j} + \hat{\mathbf{f}}_{i,j}), \mathbf{z}_i, \mathbf{m}_i), \quad (8)$$

where $\hat{\mathbf{z}}_i$ represents the enhanced latent code for the i -th frame. The mask condition \mathbf{m}_i is explicitly concatenated in the convolution blocks $\text{Conv}(\cdot)$ to improve the precision of alignment during latent code propagation.

4.3. Flow-guided Latent Interpolation

The inference in vanilla diffusion models is inefficient, which becomes even more challenging in the video domain where multiple frames need to be processed. To alleviate this issue, we propose a hypothesis: in diffusion-based

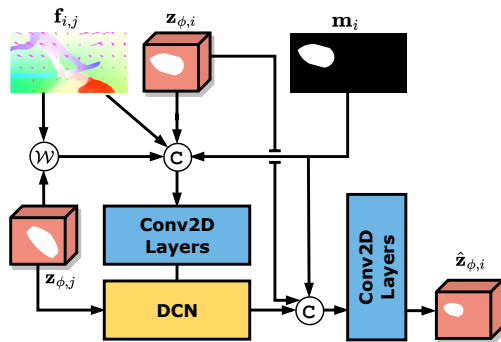


Figure 4. The process of the Flow-based Propagation.

video inpainting, adjacent frames share similar latent, aggregating them provides only *sparse* information, making it exceedingly uneconomical to infer noise for each frame at every time step. As a solution, we propose a novel flow-based latent interpolation that tailored for the VDM to release the pressure of the memory and computation burden.

As shown in Fig. 3 (along with Algorithm 1), the noisy latent code \mathbf{z} from corrupted video frames is divided into two subsets by parity. Specifically, the process entails a two-step alternating loop: even-indexed frame latents undergo denoising, whereas odd-indexed frame latents \mathbf{z}_i are obtained by interpolation using bidirectional optical flow $\mathbf{f}_{i,i+1}$ and $\mathbf{f}_{i,i-1}$, instead of denoising. In the next step, only the interpolated latents are inputted into the LDM U-Net. Owing to the negligible time cost of warping latents, the duration of diffusion denoising is halved when only half of the frame latents are processed at each sampling timestep. Notably, we solely apply adjacent frames for wrapping due to optical flow fails at long-range distances.

Ideally, we could iterate this process until latent becomes clean, but the significant artifacts arise from using down-sampled flow, which blurs spatial details, leading to poor warping outcomes. To circumvent this, we limit the interpolation to the initial S denoising steps, during which the overarching structure of the image is shaped [16]. Further more, to counter potential occlusion issues in the flow warping [13], we propose to perform the warping operation at the \mathbf{z}_0 stage (as per Equation 4), supplemented by a corrective frame-wise mask (see Algorithm 1 line 10). These strategies ensure that when occlusions are either partially or

Algorithm 1 Flow-guided Latent Interpolation

Input: Stochastic latent \mathbf{z}^T , encoded video latent \mathbf{z}_ϕ and mask sequence \mathbf{m} with N frames, completed flow \mathbf{f} , diffusion timesteps T , truncation timestamp S , U-Net of temporal LDM θ .

Output: \mathbf{z}^S

- 1: odd := {1, 3, ..., N - 1}
- 2: even := {0, 2, ..., N}
- 3: $\mathbf{i} \leftarrow$ odd **if** $T \bmod 2 = 0$ **else** even
- 4: $\bar{\mathbf{i}} := \{0, 1, \dots, N\} \setminus \mathbf{i}$
- 5: $\bar{\mathbf{z}}_\phi := \mathbf{z}_{\phi, \bar{\mathbf{i}}}$
- 6: **for** $t = T$ **to** S **do**
- 7: $\mathbf{a}^t := \mathbf{z}_{\mathbf{i}}^t$
- 8: $\bar{\mathbf{a}}^t := \mathbf{z}_{\bar{\mathbf{i}}}^t$
- 9: $\mathbf{a}^{t-1}, \epsilon_\theta \leftarrow \text{denoise}(\theta; \mathbf{a}^t, t, [\mathbf{z}_\phi; \mathbf{m}])$
- 10: $\hat{\mathbf{a}}^0 = \mathcal{P}(\mathbf{a}^t, \epsilon_\theta)$ (Eqn. 4)
- 11: $\bar{\mathbf{a}}^0 = \mathbf{m}_{\bar{\mathbf{i}}} * \mathcal{W}(\hat{\mathbf{a}}^0, \mathbf{f}) + (1 - \mathbf{m}_{\bar{\mathbf{i}}}) * \bar{\mathbf{z}}_\phi$
- 12: $\bar{\mathbf{a}}^{t-1} = \mathcal{Q}(\bar{\mathbf{a}}^0, t - 1)$ (Eqn. 1)
- 13: $\mathbf{z}^{t-1} \leftarrow \mathbf{a}^{t-1} \cup \bar{\mathbf{a}}^{t-1}$
- 14: $\mathbf{i} \leftarrow$ odd **if** $\mathbf{i} ==$ even **else** even
- 15: **end for**

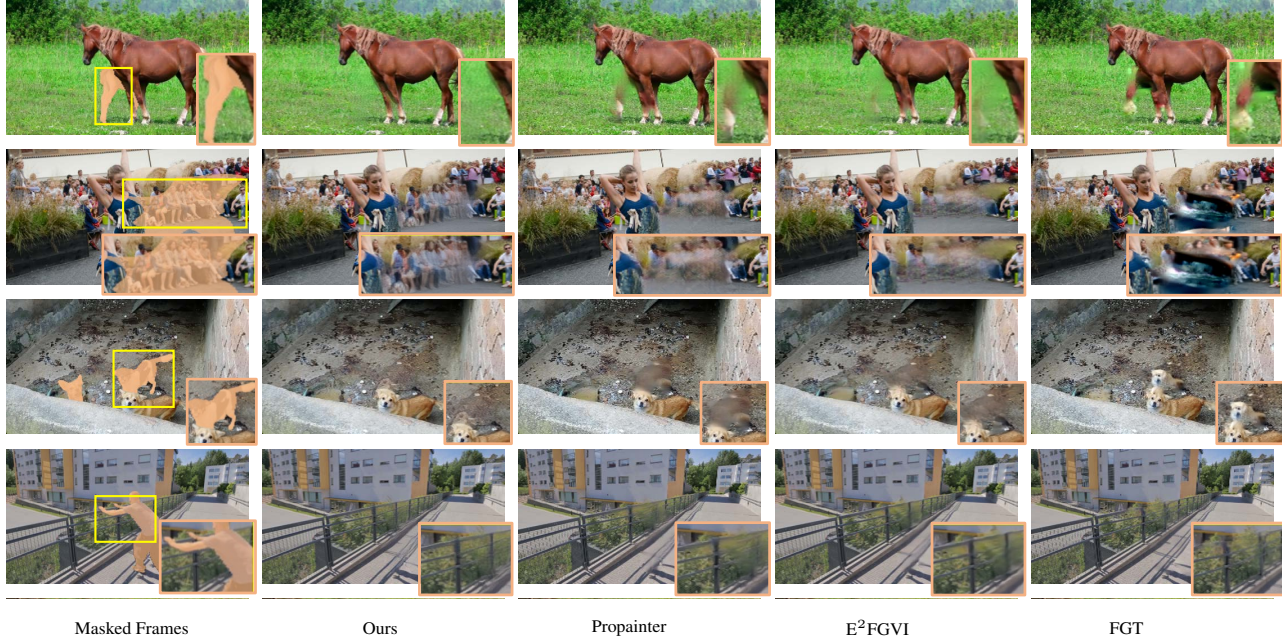


Figure 5. Qualitative comparisons with SOTA video inpainting methods. Please zoom in for better view.

Free Large Mask	MOSE [6]				DAVIS [26]			
Models	PSNR \uparrow	SSIM \uparrow	LPIPS \downarrow	$E_{warp}^* \downarrow$	PSNR \uparrow	SSIM \uparrow	LPIPS \downarrow	$E_{warp}^* \downarrow$
STTN [49]	23.08	0.8144	0.188	<u>3.31</u>	22.54	0.8069	0.169	<u>3.37</u>
DSTT [49]	25.17	0.8655	0.195	3.74	24.61	0.8639	0.153	3.82
FuseFormer [20]	25.59	0.8770	0.190	3.76	25.02	0.8761	0.145	3.87
FGT [50]	24.62	0.8628	0.176	3.60	24.94	0.8713	<u>0.106</u>	3.38
E2FGVI [18]	26.17	0.8855	<u>0.163</u>	3.31	25.57	0.8850	0.117	3.41
Propainter [54]	25.75	0.8818	0.176	3.52	<u>25.46</u>	<u>0.8853</u>	0.111	3.40
Ours	<u>25.90</u>	0.8732	0.150	3.03	25.57	0.8804	0.087	3.03
Object Seg. Mask	MOSE [6]				DAVIS [26]			
Models	PSNR \uparrow	SSIM \uparrow	LPIPS \downarrow	$E_{warp}^* \downarrow$	PSNR \uparrow	SSIM \uparrow	LPIPS \downarrow	$E_{warp}^* \downarrow$
STTN [49]	22.05	0.7956	0.188	<u>3.15</u>	21.06	0.7518	0.171	3.38
DSTT [49]	24.37	<u>0.8543</u>	0.199	3.72	22.40	0.8040	0.160	3.79
FuseFormer [20]	24.38	0.8547	0.199	3.73	22.30	0.8018	0.159	3.84
FGT [50]	24.18	0.8469	0.187	3.61	<u>22.49</u>	<u>0.8039</u>	<u>0.132</u>	3.48
E2FGVI [18]	<u>24.53</u>	0.8526	<u>0.173</u>	3.25	22.46	0.7987	0.105	2.97
Propainter [54]	24.25	0.8489	0.189	3.57	22.37	0.7989	0.134	3.42
Ours	24.58	0.8491	0.154	2.93	22.60	0.8006	0.105	2.99

Table 1. Quantitative comparisons with SOTA methods on MOSE [6] and DAVIS [26] under object removal and large free masks settings. The best two results are highlighted in bold and underline. \uparrow indicates higher is better. \downarrow indicates lower is better. E_{warp}^* denotes $E_{warp} \times 10^{-2}$.

fully encompassed by the inpainting mask, subsequent steps are optimally leveraged to enhance the final image quality. For details, see Algorithm 1. DDIM is denoted as `denoise`, and for clarity, we omit the condition c from it.

The proposed latent interpolation is a train-free strategy

designed to expedite *inference*, and can be seamlessly integrated into various VDM applications. Notably, its application during training is unnecessary, as timestamp t is randomized and cannot access the latent code from the previous timestep in the training phase.

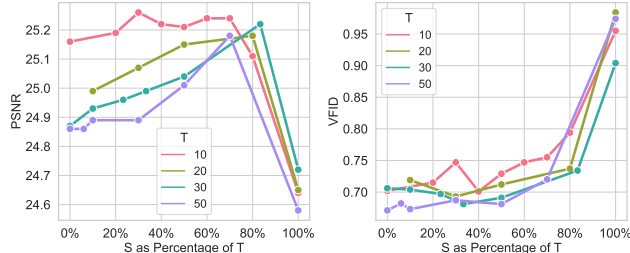


Figure 6. Ablation study of the optimal speeding step S .

5. Experiment

Datasets and Metrics. We utilize YouTube-VOS [41], comprising 3,471 and 474 video clips for training and validation, generating random shape masks with diverse motion. For evaluation, we use MOSE [6] and DAVIS [26], assessing 50 and 48 test clips, respectively. Performance is gauged using official object masks and custom large free masks, simulating complex scenarios. All video frames are resized to 256×256 for both training and evaluation. This resizing standardizes the input data, ensuring consistency across various testing conditions.

In line with prior research, we apply PSNR, SSIM [39], and LPIPS [52] for assessing reconstruction quality, alongside flow warping error E_{warp} [17] and VFID [36] to evaluate temporal consistency. These metrics collectively provide a comprehensive evaluation of the performance of our model, covering both spatial and temporal aspects of video processing.

Implementation details. For the decoupled optical flow completion module, we train it on the 256×256 resolution and input a flow sequence of length 10, while running for $70K$ iterations on two TITAN XP GPU(12G) cards with a batch size of 5. We adopt the Ranger optimizer [40] with initial learning rate of 0.00005. As shown in Fig. 2, during training, the latent propagation latent is jointly trained with diffusion model, where flow completion module is fixed. We set the input to be video clips of length 4 concatenated with 5 reference frames, and only local video clips are improved by propagation. Besides, we leverage the Adam [15] optimizer with initial learning rate of 0.0001 while running



Figure 7. Visualization of the flow-guided latent interpolation.

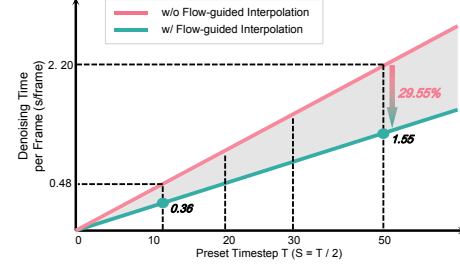


Figure 8. Flow-guided latent interpolation efficiency at $S = T/2$.

$70K$ iterations on three Tesla V100 GPU(32G) cards with a batch size of 1. Considering the DDIM sampling, we set $S = 5, T = 10$ for all our experiments. This training approach, with its distinct phase separation and resource allocation, ensures optimal learning and efficiency.

5.1. Comparison

Quantitative comparisons. We conducted a comprehensive comparison of our FGDVI method with six leading-edge approaches, namely Propainter [54], E²FGVI [18], FGT [50], FuseFormer [20], DSTT [49], and STTN [49]. The evaluations were performed on the MOSE [6] and DAVIS [26] datasets. To realistically represent scenarios such as object removal, our analysis initially focused on using the official object masks from MOSE and DAVIS. Additionally, we introduced stationary, extensive free masks to replicate more complex situations, as detailed in Table 1. The quantitative assessments were executed under identical conditions, employing a neighbor window of size 5 and a reference distance of 12. Despite the inherent disadvantage of resizing other state-of-the-art methods, which were trained at a resolution of 432×240 , to 256×256 , our findings indicate that FGDVI outperforms these methods significantly. As evidenced in Table 1, FGDVI exhibits superior performance in PSNR in object removal scenarios and yields impressive results in settings involving large masks. Moreover, FGDVI consistently excels in LPIPS across all comparative analyses. Regarding temporal consistency, FGDVI demonstrates enhanced outcomes in E_{warp} , marking a substantial improvement of 10%. These results underscore FGDVI's exceptional proficiency in video inpainting, achieving higher quality and improved consistency.

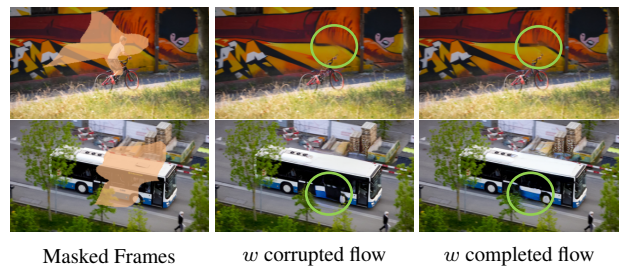


Figure 9. Effectiveness of the completed optical flow.

Case	PSNR↑	SSIM↑	VID ↓
w/o optical flow	25.16	0.8687	0.700
w/ corrupted flow	25.42	0.8778	0.690
w/ completed flow	26.11	0.8948	0.588
w/ gt flow	26.12	0.8950	0.563

Table 2. Effectiveness of flow completion module.

Qualitative comparison. For the quantitative comparison, we compare FGDVI with three flow-guided frameworks that based on transformer, including Propainter [54], E²FGVI [18] and FGT [50]. The qualitative comparisons are conducted under the same setting for inference. As shown in Fig. 5 and Fig. 11, FGT [50] leads to enormous artifacts within the the missing region under condition of large free masks at line 2nd. While E²FGVI [18] and Propainter [54] generates the blurry results, which lack enough details at lines 3rd and 6th. Besides, they fails to accomplish inpainting both under complex situations and object removal at lines 2nd and 4th. In contrast, FGDVI synthesizes more realistic results regardless of the conditions, which verifies the superiority of it over SOAT solutions. Specifically, FGDVI recoveries the crowd at line 2nd as much as possible without pronounced artifacts under the large free mask setting. Meanwhile, it also manages to produce the convincing results under the object removal setting, such as the leg of the horse at lines 1st, vivid texture at line 3th, and iron railings at line 4th, where it seems difficult for other SOTA methods. For further examples, see appendix video demos.

5.2. Ablation Study

Speeding Steps. In order to find the optimal value of latent interpolation step S , we conducted experiments on PSNR and VFID to illustrate the performance’s variation when S changes from 0 to T . When $S = 0$, there is no latent interpolation involved, and in contrast, $S = T$ means we expedite the whole diffusion sampling process. As the Fig. 6 exhibits, PSNR will rise steadily to the peak till it comes to the 80% of T , while the VFID also shows the sim-

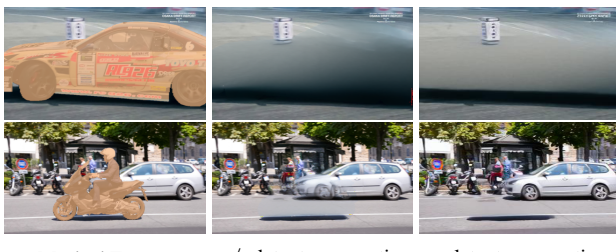


Figure 10. Ablation studies of latent propagation module.

Case	PSNR ↑	SSIM ↑	VID ↓
LDM	20.13	0.7440	1.188
w/ spatial attention	22.96	0.8107	0.895
w/o latent propagation	25.16	0.8687	0.700
FGDVI	26.11	0.8948	0.588

Table 3. Ablation study of the attention mechanism.

ilar tendency. Therefore, we choose $S = T/2$, especially $S = 5, T = 10$ as the basic setting for all our experiments. As shown in Fig. 7, under this condition, flow-guided interpolation has a positive effect in terms of refinement. The qualitative and quantitative results both demonstrate latent interpolation achieving two birds with one stone: when it accelerates the denosing process, the performance on both inpainting quality and temporal consistency of FGDVI are naturally improved.

Efficiency analysis. In order to demonstrate the effectiveness of our proposed flow-guided latent interpolation method for the diffusion model, we calculate the per-frame sampling time under the speeding steps $S = T/2$ from $T = 10$ to 50. As displayed in Fig. 8, when $T = 50$, compared to the vanilla diffusion baseline, our approach significantly boosts inference speed by approximately **29%**, which can be seamlessly integrated into any various video diffusion model applications without any training.

Study of decoupled flow completion module. In Tab. 2, we compare different flow conditions for latent propagation, which evidences the effectiveness of our decoupled flow completion module. Besides, Fig. 9 displays the representative results under different flow conditions, which also prove the strength of flow completion module.

Study of latent propagation module. To examine the improvement of the one-step latent propagation module, we directly use the origin masked video latent \mathbf{z}_ϕ without latent propagation to concatenate with the binary masks \mathbf{m} and stochastic latent code \mathbf{z}_0 as the LDM’s input. As shown in Fig. 10, under the enhancement of the optical flows, FGDVI has a better performance in processing temporal cues when large movements occur. The comparison between the 2st and the 4st line of Tab. 2 also indicates the superiority of our latent propagation module.

Study of spatiotemporal attention mechanism. For purpose of unlocking the capabilities of the pretrained image diffusion model for video, we extend vanilla attentions to the spatiotemporal domain, the results in Tab. 3 verify its huge improvement on the inpainting quality (PSNR) and temporal consistency (VFID).

6. Conclusions

In this work, we are the first to reveal the effectiveness of a diffusion-based method in video inpainting. Our proposed FGDVI leverages optical flow to notably improve inpainting quality and temporal consistency. Besides, we introduce model-agnostic flow-guided latent interpolation method to expedite denoising sampling process, which can be seamlessly integrated into any other Video Diffusion Model applications without any training. As a baseline of video inpainting diffusion model, extensive experiments show our method's superiority in complex situations compared to SOTA methods.

For sake of the traditional video inpainting, we temporarily employ a pre-trained LDM instead of the Stable Diffusion's [1], where U-Net contain cross attention layer for text input. But in the future, we aims at adding text modal as input with more powerful SD as diffusion model. Besides, for pursuing better temporal consistency, we leverage adjacent frames for flow-based interpolation. But in the future, we plan to design a more challenge algorithm with fewer key frames, while bringing greater improvements.

References

- [1] *Stable Diffusion v2*, 2022. <https://huggingface.co/stabilityai/stable-diffusion-2-depth>. 9
- [2] Jie An, Songyang Zhang, Harry Yang, Sonal Gupta, Jia-Bin Huang, Jiebo Luo, and Xi Yin. Latent-shift: Latent diffusion with temporal shift for efficient text-to-video generation. *CoRR*, abs/2304.08477, 2023. 3
- [3] Omri Avrahami, Ohad Fried, and Dani Lischinski. Blended latent diffusion. *ACM Trans. Graph.*, 2023. 4
- [4] Andreas Blattmann, Robin Rombach, Huan Ling, Tim Dockhorn, Seung Wook Kim, Sanja Fidler, and Karsten Kreis. Align your latents: High-resolution video synthesis with latent diffusion models. In *CVPR*, pages 22563–22575. IEEE, 2023. 2
- [5] Hyungjin Chung, Byeongsu Sim, and Jong Chul Ye. Come-closer-diffuse-faster: Accelerating conditional diffusion models for inverse problems through stochastic contraction. In *CVPR*, 2022. 2
- [6] Henghui Ding, Chang Liu, Shuting He, Xudong Jiang, Philip H. S. Torr, and Song Bai. MOSE: A new dataset for video object segmentation in complex scenes. *CoRR*, abs/2302.01872, 2023. 6, 7
- [7] Mounira Ebdelli, Olivier Le Meur, and Christine Guillemot. Video inpainting with short-term windows: Application to object removal and error concealment. *IEEE Trans. Image Process.*, 2015. 1
- [8] Fanda Fan, Chaoxu Guo, Litong Gong, Biao Wang, Tiezheng Ge, Yuning Jiang, Chunjie Luo, and Jianfeng Zhan. Hierarchical masked 3d diffusion model for video outpainting. In *ACM MM*, 2023. 3
- [9] Chen Gao, Ayush Saraf, Jia-Bin Huang, and Johannes Kopf. Flow-edge guided video completion. In *ECCV*, 2020. 2
- [10] Jonathan Ho and Tim Salimans. Classifier-free diffusion guidance. *CoRR*, abs/2207.12598, 2022. 1
- [11] Jonathan Ho, Ajay Jain, and Pieter Abbeel. Denoising diffusion probabilistic models. In *NeurIPS*, 2020. 1, 2, 3
- [12] Jonathan Ho, Tim Salimans, Alexey A. Gritsenko, William Chan, Mohammad Norouzi, and David J. Fleet. Video diffusion models. In *NeurIPS*, 2022. 2
- [13] Zhihao Hu and Dong Xu. Videocontrolnet: A motion-guided video-to-video translation framework by using diffusion model with controlnet. *CoRR*, abs/2307.14073, 2023. 5
- [14] Jaeyeon Kang, Seoung Wug Oh, and Seon Joo Kim. Error compensation framework for flow-guided video inpainting. In *ECCV*, 2022. 2
- [15] Diederik P. Kingma and Jimmy Ba. Adam: A method for stochastic optimization. In *ICLR*, 2015. 7
- [16] Mingi Kwon, Jaeseok Jeong, and Youngjung Uh. Diffusion models already have A semantic latent space. In *ICLR*, 2023. 5
- [17] Wei-Sheng Lai, Jia-Bin Huang, Oliver Wang, Eli Shechtman, Ersin Yumer, and Ming-Hsuan Yang. Learning blind video temporal consistency. In *ECCV*, 2018. 2, 7
- [18] Zhen Li, Chengze Lu, Jianhua Qin, Chun-Le Guo, and Ming-Ming Cheng. Towards an end-to-end framework for flow-guided video inpainting. In *CVPR*, 2022. 1, 2, 4, 5, 6, 7, 8
- [19] Jun Hao Liew, Hanshu Yan, Jianfeng Zhang, Zhongcong Xu, and Jiashi Feng. Magicedit: High-fidelity and temporally coherent video editing. *CoRR*, abs/2308.14749, 2023. 3
- [20] Rui Liu, Hanming Deng, Yangyi Huang, Xiaoyu Shi, Lewei Lu, Wenxiu Sun, Xiaogang Wang, Jifeng Dai, and Hongsheng Li. Fuseformer: Fusing fine-grained information in transformers for video inpainting. In *ICCV*, 2021. 1, 2, 6, 7
- [21] Rui Liu, Hanming Deng, Yangyi Huang, Xiaoyu Shi, Lewei Lu, Wenxiu Sun, Xiaogang Wang, Jifeng Dai, and Hongsheng Li. Decoupled spatial-temporal transformer for video inpainting. *CoRR*, abs/2104.06637, 2021. 2
- [22] Cheng Lu, Yuhao Zhou, Fan Bao, Jianfei Chen, Chongxuan Li, and Jun Zhu. Dpm-solver: A fast ODE solver for diffusion probabilistic model sampling in around 10 steps. In *NeurIPS*, 2022. 2
- [23] Alasdair Newson, Andrés Almansa, Matthieu Fradet, Yann Gousseau, and Patrick Pérez. Video inpainting of complex scenes. *CoRR*, 2015. 1
- [24] Alexander Quinn Nichol, Prafulla Dhariwal, Aditya Ramesh, Pranav Shyam, Pamela Mishkin, Bob McGrew, Ilya Sutskever, and Mark Chen. GLIDE: towards photorealistic image generation and editing with text-guided diffusion models. In *ICML*, 2022. 1
- [25] Hao Ouyang, Tengfei Wang, and Qifeng Chen. Internal video inpainting by implicit long-range propagation. In *ICCV*, 2021. 1
- [26] Federico Perazzi, Jordi Pont-Tuset, Brian McWilliams, Luc Van Gool, Markus H. Gross, and Alexander Sorkine-Hornung. A benchmark dataset and evaluation methodology for video object segmentation. In *CVPR*, 2016. 6, 7

[27] Dustin Podell, Zion English, Kyle Lacey, Andreas Blattmann, Tim Dockhorn, Jonas Müller, Joe Penna, and Robin Rombach. SDXL: improving latent diffusion models for high-resolution image synthesis. *CoRR*, abs/2307.01952, 2023. 1

[28] Anurag Ranjan and Michael J. Black. Optical flow estimation using a spatial pyramid network. In *CVPR*, 2017. 4

[29] Alex Rogozhnikov. Einops: Clear and reliable tensor manipulations with einstein-like notation. In *ICLR*, 2022. 3

[30] Robin Rombach, Andreas Blattmann, Dominik Lorenz, Patrick Esser, and Björn Ommer. High-resolution image synthesis with latent diffusion models. In *CVPR*, 2022. 1, 2, 3

[31] Hao Shi, Qi Jiang, Kailun Yang, Xiaoting Yin, and Kaiwei Wang. Flowlens: Seeing beyond the fov via flow-guided clip-recurrent transformer. *CoRR*, abs/2211.11293, 2022. 4

[32] Uriel Singer, Adam Polyak, Thomas Hayes, Xi Yin, Jie An, Songyang Zhang, Qiyuan Hu, Harry Yang, Oron Ashual, Oran Gafni, Devi Parikh, Sonal Gupta, and Yaniv Taigman. Make-a-video: Text-to-video generation without text-video data. In *ICLR*, 2023. 2

[33] Jiaming Song, Chenlin Meng, and Stefano Ermon. Denoising diffusion implicit models. In *ICLR*, 2021. 1, 2

[34] Nick C. Tang, Chiou-Ting Hsu, Chih-Wen Su, Timothy K. Shih, and Hong-Yuan Mark Liao. Video inpainting on digitized vintage films via maintaining spatiotemporal continuity. *IEEE Trans. Multim.*, 2011. 1

[35] Su Wang, Chitwan Saharia, Ceslee Montgomery, Jordi Pont-Tuset, Shai Noy, Stefano Pellegrini, Yasumasa Onoe, Sarah Laszlo, David J. Fleet, Radu Soricut, Jason Baldridge, Mohammad Norouzi, Peter Anderson, and William Chan. Imagen editor and editbench: Advancing and evaluating text-guided image inpainting. In *CVPR*, 2023. 1

[36] Ting-Chun Wang, Ming-Yu Liu, Jun-Yan Zhu, Nikolai Yakovenko, Andrew Tao, Jan Kautz, and Bryan Catanzaro. Video-to-video synthesis. In *NeurIPS*, 2018. 7

[37] Wenjing Wang, Huan Yang, Zixi Tu, Huiguo He, Junchen Zhu, Jianlong Fu, and Jiaying Liu. Videofactory: Swap attention in spatiotemporal diffusions for text-to-video generation. *arXiv preprint arXiv:2305.10874*, 2023. 1

[38] Xiang Wang, Hangjie Yuan, Shiwei Zhang, Dayou Chen, Jiumiu Wang, Yingya Zhang, Yujun Shen, Deli Zhao, and Jingen Zhou. Videocomposer: Compositional video synthesis with motion controllability. *CoRR*, abs/2306.02018, 2023. 3

[39] Zhou Wang, Alan C. Bovik, Hamid R. Sheikh, and Eero P. Simoncelli. Image quality assessment: from error visibility to structural similarity. *IEEE Trans. Image Process.*, 2004. 7

[40] Less Wright. Ranger - a synergistic optimizer. <https://github.com/lessw2020/Ranger-Deep-Learning-Optimizer>, 2019. 7

[41] Ning Xu, Linjie Yang, Yuchen Fan, Jianchao Yang, Dingcheng Yue, Yuchen Liang, Brian L. Price, Scott Cohen, and Thomas S. Huang. Youtub-e-vos: Sequence-to-sequence video object segmentation. In *ECCV*, 2018. 7

[42] Rui Xu, Xiaoxiao Li, Bolei Zhou, and Chen Change Loy. Deep flow-guided video inpainting. In *CVPR*, 2019. 2, 4, 5

[43] Jiahui Yu, Zhe Lin, Jimei Yang, Xiaohui Shen, Xin Lu, and Thomas S. Huang. Free-form image inpainting with gated convolution. In *ICCV*, 2019. 1

[44] Sihyun Yu, Kihyuk Sohn, Subin Kim, and Jinwoo Shin. Video probabilistic diffusion models in projected latent space. In *CVPR*, 2023. 3

[45] Yongsheng Yu, Dawei Du, Libo Zhang, and Tiejian Luo. Unbiased multi-modality guidance for image inpainting. In *ECCV*, 2022. 1

[46] Yongsheng Yu, Libo Zhang, Heng Fan, and Tiejian Luo. High-fidelity image inpainting with GAN inversion. In *ECCV*, 2022. 1

[47] Yongsheng Yu, Heng Fan, and Libo Zhang. Deficiency-aware masked transformer for video inpainting. *arXiv preprint arXiv:2307.08629*, 2023. 1

[48] Yongsheng Yu, Hao Wang, Tiejian Luo, Heng Fan, and Libo Zhang. Magic: Multi-modality guided image completion. *CoRR*, abs/2305.11818, 2023. 1

[49] Yanhong Zeng, Jianlong Fu, and Hongyang Chao. Learning joint spatial-temporal transformations for video inpainting. In *ECCV*, 2020. 1, 2, 6, 7

[50] Kaidong Zhang, Jingjing Fu, and Dong Liu. Flow-guided transformer for video inpainting. In *ECCV*, 2022. 1, 2, 4, 5, 6, 7, 8

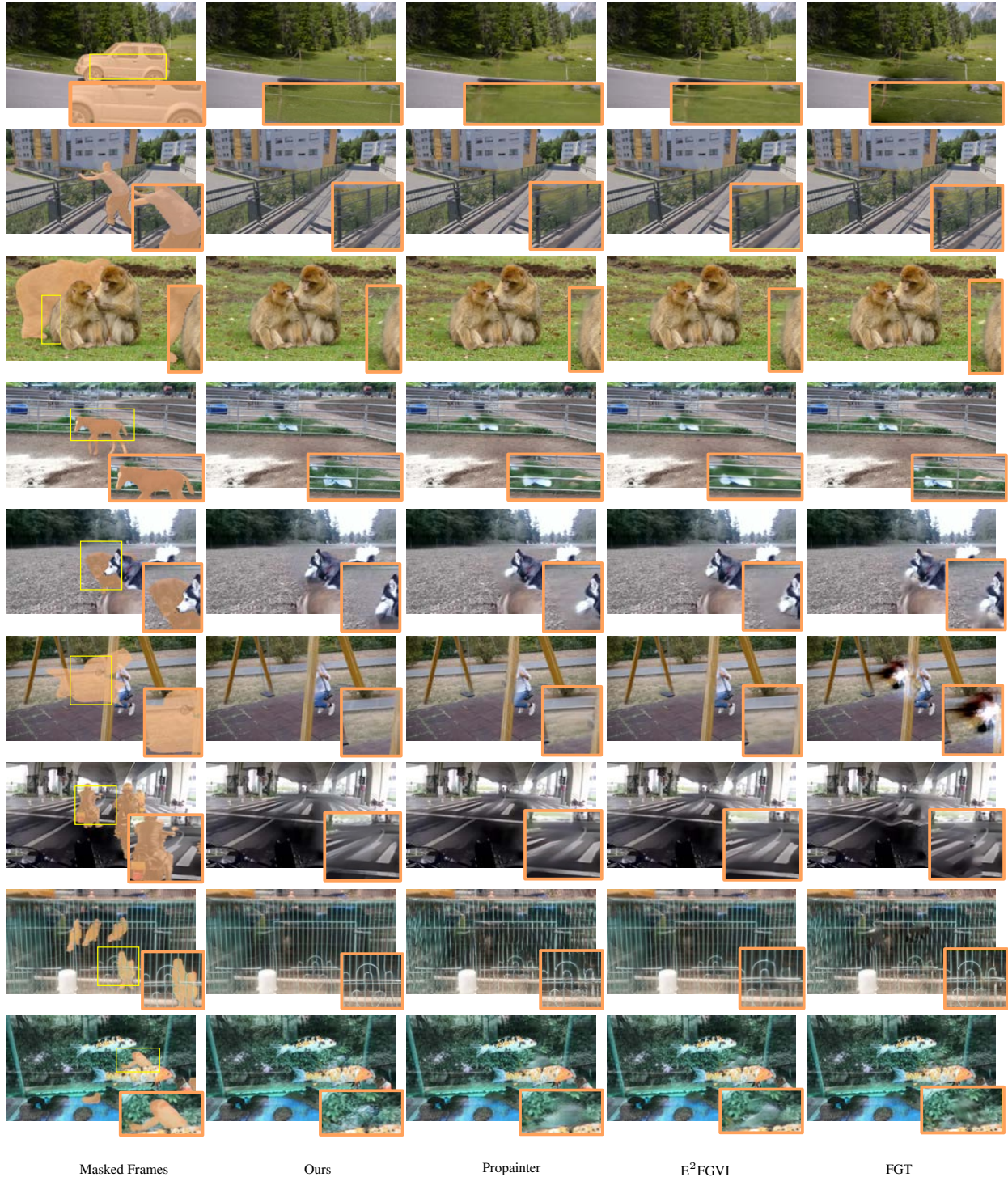
[51] Lvmin Zhang and Maneesh Agrawala. Adding conditional control to text-to-image diffusion models. *CoRR*, abs/2302.05543, 2023. 1

[52] Richard Zhang, Phillip Isola, Alexei A. Efros, Eli Shechtman, and Oliver Wang. The unreasonable effectiveness of deep features as a perceptual metric. In *CVPR*, 2018. 7

[53] Daquan Zhou, Weimin Wang, Hanshu Yan, Weiwei Lv, Yizhe Zhu, and Jiashi Feng. Magicvideo: Efficient video generation with latent diffusion models. *CoRR*, abs/2211.11018, 2022. 3

[54] Shangchen Zhou, Chongyi Li, Kelvin C. K. Chan, and Chen Change Loy. Propainter: Improving propagation and transformer for video inpainting. *CoRR*, abs/2309.03897, 2023. 1, 2, 4, 5, 6, 7, 8

[55] Junchen Zhu, Huan Yang, Wenjing Wang, Huiguo He, Zixi Tu, Yongsheng Yu, Wen-Huang Cheng, Lianli Gao, Jingkuan Song, Jianlong Fu, et al. Mobilevidfactory: Automatic diffusion-based social media video generation for mobile devices from text. In *ACM MM*, pages 9371–9373, 2023. 1



Masked Frames

Ours

Propainter

E^2 FGVI

FGT

Figure 11. More qualitative comparison with SOTA video inpainting methods. Please zoom in for better view.